

1 Relationships of biomass burning aerosols with
2 precipitation and cloud properties in Australia

3 Jennifer D. Small, Jonathan H. Jiang and Hui Su

4 October 14, 2010

5 California Institute of Technology, Jet Propulsion Laboratory, 4800 Oak Grove Drive,
6 Pasadena, CA 91109

7 Corresponding Author:
8 Jennifer D. Small
9 Jet Propulsion Laboratory
10 California Institute of Technology
11 4800 Oak Grove Dr.
12 Pasadena, CA 91109
13 Phone: 818-354-0603
14 Fax: 818-393-5065
15 email: jennifer.d.small@jpl.nasa.gov

16 © Copyright 2010. All rights reserved.

Abstract

19 Understanding the complex interactions between aerosol, clouds, and precipitation
20 is an important and necessary step towards understanding the climate system and the
21 development of accurate global and regional climate models. Documented aerosol ef-
22 fects on clouds and precipitation are not homogeneous over the globe. Here, we study
23 the relationships between aerosols, cloud and precipitation over both land and ocean for
24 the north coastal Australia and Indonesian region (INC) and the south coastal Australia
25 and New Zealand region (NZSC). We use data from long-term multi-satellite observa-
26 tions including Nimbus 7-TOMS, Earth Probe-TOMS and Aura-OMI Aerosol Index,
27 Global Precipitation Climatology Project precipitation, Aqua-MODIS fire counts, ef-
28 fective radius of liquid clouds and cloud fraction and mean cloud amount from the
29 International Satellite Cloud Climatology Project. The long-term data sets reveal clear
30 regional differences and distinct inter-decadal and inter-annual variations in aerosol
31 loading and precipitation amount. For both the INC and NZSC regions we find that
32 aerosol shows positive correlations with fire occurrence and negative correlations with
33 precipitation, cloud fraction and liquid cloud effective radius. The strength of the rela-
34 tionships are regionally dependent with the INC showing the stronger correlations than
35 the NZSC.

1 Introduction

In both theoretical and observational studies, microphysical properties of clouds are found to be influenced by atmospheric aerosol loading. For example, there is ample evidence of the first-indirect effect (*Twomey, 1974*) with an increase in cloud number concentration with increasing aerosol concentration in both cumuli- and stratiform clouds (*Ramanathan et al., 2001*). As aerosol concentration is varied the width of the drop size distribution also changes, with clean clouds having broader size distributions than their polluted counterparts in both continental (*Martins and Silva Dias, 2009*) and maritime conditions (*Pawlowska et al., 2006*). Recent studies find a general decrease in effective radius with increased aerosol concentrations (*Wyser, 1998; Lu et al., 2008; Jiang et al., 2010*). For a more complete discussion of cloud-aerosol interactions see *Feingold and Siebert (2009)*.

Nearly 50 years ago *Gunn and Phillips (1957)*, through simple laboratory experiments, found that aerosols have important microphysical effects and that air pollution could cause a reduction in precipitation by slowing the conversion of cloud drops into raindrops. The natural system, however, has proved to be more complex and there has been much recent debate regarding the effect of aerosol on precipitation (e.g. *Rosenfeld et al. 2008*). According to the IPCC 4th assessment report (*Denman et al., 2007*), the global precipitation change attributable to aerosol is unclear. Some studies report suppression of precipitation (*Rosenfeld, 1999; Andreae et al., 2004; Jiang et al., 2008; Huang et al., 2009b; Graf et al., 2009*) while others report an enhancement of precipitation (*Andreae et al., 2004; Lin et al., 2006; Bell et al., 2008; Zhang et al., 2007*) with increasing aerosol concentrations. These conflicting results are due, in part, to the regional nature of aerosols, differences in cloud types (e.g. warm vs. cold clouds) and variations due to meteorology and dynamics.

Due to the regional nature of aerosols, precipitation and fire occurrence it is necessary to focus on locations within specific dynamic and meteorological regimes. Thus, this work provides an analysis of two dynamically different study regions in Australia, a tropical convective region (INC) strongly influenced by monsoons and a subtropical region (NZSC) with

weak seasonality. Biomass burning, in the form of bushfires and wildfires, are a common occurrence in Australian ecosystems and landscapes. In northern coastal regions bushfires are most common over the savannas where some parts of the land burn annually. The southern coastal regions, including the southeast where the majority of Australia’s population resides, are susceptible to large wildfires (*Hennessey et al.*, 2005). These fires are the result of both natural causes such as lightning during the transition from dry to wet seasons and anthropogenic events, accidental and deliberate, throughout the dry season (*Bowman and Wilson*, 1988). Recent studies suggest an increasing trend in fire season length, especially for southeast Australia for the last decade (*Lucas et al.*, 2007). Increased fire season length may lead to more intense fires, increased number of fires or increased aerosol input into the atmosphere.

Spatial (area burned) and temporal (decadal, inter-annual, and annual) variations of biomass burning occurrence complicate investigations into aerosol effects on clouds and precipitation. Mechanisms thought to affect the annual and inter-annual variability of fire in Australia include El Niño-Southern Oscillation (ENSO) (*Nicholls*, 1989), Indian Ocean Dipole (IOD) (*Saji et al.*, 1999), and Southern Annular Mode (SAM) (*Hendon et al.*, 2007). These climate signals drastically affect precipitation over Australian continent and must thus be taken into consideration when analyzing the relationships among aerosol, precipitation and clouds. Additionally, the Australian continent is prone to extensive droughts on the order of a decade or more in length (*Ummenhofer et al.*, 2009a; *Verdon-Kidd and Kiem*, 2009) which are related to above-normal fire potential (*Murphy and Timbal*, 2008).

This analysis combines observations of aerosol, clouds and precipitation from both historical and recent satellite sensors, described in detail in Section 3. Using both historical and recent data records we can address many unanswered questions related to aerosol, clouds and precipitation. How does atmospheric aerosol loading change on annual, inter-annual and decadal timescales in the Australian region and how does it relate to the history of fire occurrence. How do cloud properties, including effective radius, cloud fraction and mean cloud

amount, relate to aerosol loading in the two study regions? How has Australian precipitation varied for the same timescales and in relation to changes in cloud properties?

In this work we introduce the study regions in Section 2, describe the data Section 3, present our results in Section 4, and provide a summary and discussion of the work in Section 5.

2 Study Regions

The two main study regions are outlined by black boxes in Figure 1. The Indonesia and northern coast region (INC), is dominated by woodland and open forests, while the New Zealand and southern coast (NZSC) region is dominated by woodland, scrub land and heath (*Specht*, 1970). In general, main Australian aerosol contributions include biomass burning, primarily in coastal regions, and dust in the center of the continent. To avoid the majority of the desert dust aerosol the two study regions exclude central Australia. Note that there is still dust present in the aerosol observations for the NZSC due to its proximity to the central desert region and the general circulation pattern over the continent. There is limited input from anthropogenic sources in the INC region and the center of the continent due to the dearth of large cities and a low mean population density. The main population centers (e.g. Sydney and Melbourne) are located in the eastern portion of the NZSC region adding additional anthropogenically generated aerosol.

3 Data

This study utilizes nearly 30 years of monthly averaged data collected with various satellite born instrumentation observing aerosols, clouds and precipitation over both land and ocean. This allows for the analysis of their relationships on decadal, inter-annual and annual time scales.

To obtain a historical perspective of aerosol index we use the Nimbus-7 Total Ozone

Mapping Spectrometer (TOMS) data from November 1978 to April 1993 and the Earth Probe TOMS for the period July 1996 through November 2001 (*Torres et al.*, 1998, 2002). Data after 2001 for the EP TOMS are excluded due to instrumental issues (O. Torres, *personal communication*). It is the first instrument to allow observation of aerosols as the particles cross the land/sea boundary (*Hsu et al.*, 1996; *Herman et al.*, 1997). Using these data it is possible to observe a wide range of phenomena such as desert dust storms, forest fires and biomass burning. The Global Precipitation Climatology Project (GPCP) Version 2.1 Combined Precipitation Data Set, (*Huffman et al.*, 2009), with a record spanning January 1979 to December 2009 and mean cloud amount (MCA) from the International Satellite Cloud Climatology Project (ISCCP) from July 1983 to June 2008, (*Rossow and Schiffer*, 1991, 1999), provide long-term historical estimations of precipitation and cloud properties. For the GPCP record, monthly means are the product of combined geosynchronous-orbit satellite observations and rain-gage data from weather stations. Data was converted from $2.5^{\circ} \times 2.5^{\circ}$ global grid to $1^{\circ} \times 1.25^{\circ}$ grid to match TOMS data. ISCCP data are converted from an Equal-Area grid format to $1^{\circ} \times 1.25^{\circ}$ format for ease of comparison with all other datasets.

For the contemporary period we use aerosol index data from the Ozone Monitoring Instrument (OMI), (*Levelt et al.*, 2006), for October 2004 through May 2008, and aerosol optical depth (AOD) data from the Moderate Resolution Imaging Spectroradiometer (MODIS) for July 2002 to April 2010, (*Chu et al.*, 2002; *Remer et al.*, 2002; *Chu et al.*, 2003; *Kaufman et al.*, 1997). Both OMI and MODIS data sets have been re-gridded from a $1^{\circ} \times 1^{\circ}$ grid to $1^{\circ} \times 1.25^{\circ}$ to match the TOMS data. In addition to MODIS AOD, we also include liquid cloud effective radius (r_e), cloud fraction (CF), and fire counts from MODIS to expand our contemporary analysis. We use MODIS fire count data to identify periods of bushfire activity, keeping in mind that these measurements refer to number of fires rather than intensity of fires.

As mentioned in Section 1 ENSO, IOD, and SAM are climate factors known to modulate natural variability of aerosol and precipitation. We use the Niño 3.4 index (*Reynolds and*

Smith, 1994), IOD index (*Saji et al.*, 1999), SAM index (*Marshall*, 2003) for the time period of November 1978 through May 2008 in a linear regression analysis to remove their signals from the aerosol, cloud and precipitation data sets. This method is described in detail in Section 4.3.

4 Results

4.1 Decadal variations

Figure 2 shows the mean timeseries of TOMS/OMI AI, GPCP precipitation, and the three climate indices. In Figure 2a we see a general increase in aerosol loading over the entire record (Table 2), with the greatest increase seen from November 1978 to the end of the N7 record in 1993 and additional increases during the EP TOMS and OMI records. For the INC region AI values have increased by 0.05 over the whole record while AI values in the NZSC have increased by 0.11 during the study time period (Table 2). The N7 and EP TOMS records show that the INC region has higher aerosol loading than the NZSC region. In the OMI record we see that the mean aerosol loading in the NZSC region exceeds that of the INC. This indicates that aerosol production in the NZSC has been increasing more than in the INC region over the last decade. This is not unexpected due to the prolonged drought affecting southeast Australia since the mid-1900s (*Verdon-Kidd and Kiem*, 2009; *Murphy and Timbal*, 2008) and an observed increase in aerosol loading over the Australian arid zone (*Mitchell et al.*, 2010). We also see a clear seasonal cycle of precipitation, for both the INC and NZSC regions (Figure 2b). The INC shows more inter-annual variability than the NZSC, annual means and standard deviations are higher (14.1 ± 10.6 cm/month) than those for the NZSC (7.1 ± 3.6 cm/month). As expected, for both regions peaks in Nino3.4, IOD and SAM, Figure 2c, d and e respectively, correspond to periods of decreased precipitation and increased aerosol (*Taschetto and England*, 2009; *Ummenhofer et al.*, 2009b; *Hendon et al.*, 2007).

4.2 Annual variations

Spatial climatologies and annual cycles of fire count, aerosol, cloud fraction and precipitation are documented in Figure 3. Figure 3a shows average fire counts for the ~ 8 year MODIS record with maximum average fire counts occurring along the northern coast in the INC region. We also see a concentration of fires in the eastern region of the NZSC, though smaller in number than in the north. Note that MODIS fire count only measures number and not intensity. The annual cycles in Figure 3b reveal that the main bushfire season for the INC is September-November and November-February for the NZSC. This is a result of the gradual traverse of the sun from tropical to sub-tropical latitudes as the seasons progress.

The climatological aerosol maximum is located in the center of the Australian continent, mainly in the proximity of the Simpson Desert, while the aerosol minimum is located near the west coast of Australia. The main aerosol season for the INC region is September-November, associated with biomass burning from bushfires (see maximum fire count in Figure 3b), and is clearly identified in Figure 3c as well as the AI minimum in May-August. For the NZSC region the peak aerosol occurs in May-August, associated primarily with dust transport from the central desert (*Marx et al.*, 2005). The 30 year averaging conceals a separate aerosol peak which occurs during the NZSC region fire season in November-February (to be discussed later).

Maximums in CF are located primarily over the ocean outside of the main region of subsidence around 30°S . Peak CF occurs in the tropics as a result of the inter-tropical convergence zone while peak CF in the NZSC is a result of southern ocean storm fronts and clouds formed due to large scale subsidence (i.e. ocean stratocumulus). We see a minimum of CF over the continent with an interesting minimum off the western coast, located close to the main fire region of the INC in an area of aerosol outflow, clearly seen in Figure 3a and c. The annual cycle of CF shows a general anti-correlation with fire count, primarily for the INC, when fire counts are high and cloud fractions are low.

The precipitation maximum, associated with the inter-tropical convergence zone and

monsoonal flow (*Gentili*, 1971), is located in the INC region in the Indonesian Through-flow and the precipitation minimum is found over the central deserts in Australia and along 30°S over the Indian Ocean. The eastern coast experiences more rainfall than its western counterpart, partially due to the west coasts cold-upwelling currents and low evaporation rates. The annual cycle of precipitation shows a minimum in July-September for the INC region and in November-February for the NZSC region; maximum precipitation occurs from December-March in the INC region and in May-July in the NZSC region.

In Figure 3a, c, e and g we see that maximum AI values, minimum fire counts and minimum precipitation values are primarily associated with the Simpson desert in central Australia. Similarly, maximum fire counts correspond to local highs in AI and minimums in CF and precipitation. Interestingly, in the case of the western portion of the INC region, considerable land-to-ocean transport of aerosol is evident. The annual timing of fire, aerosol and cloud properties and how they are related will be addressed in the Section 4.4.

4.3 Inter-annual variations

In order to reduce the expected meteorological effects on clouds and precipitation within each dynamic regime, we average over a large number of samples such that both the INC and NZSC regions are characterized by adequate precipitation amounts, aerosol loading, and fire counts. We follow the data processing methods presented by *Huang et al.* (2009a) to remove seasonal cycles and climate factors. After identifying the INC and NZSC regions mean monthly and yearly timeseries of all the data sets described in Section 3 are computed for each region. Climatological seasonal cycles are then removed to obtain a time series of normalized anomalies for each satellite. For example, only Nimbus-7 TOMS is used in computing the Nimbus-7 TOMS normalized anomalies. To calculate the normalized anomalies a record mean and standard deviation for each satellite is determined. The monthly means are then subtracted from each calendar month and the resulting anomaly is then divided by the appropriate monthly standard deviation. We use multiple-linear regression to remove the

variability of fire counts, aerosol (TOM, OMI AI and MODIS AOD), precipitation (GPCP), and cloud properties (r_e , CF and MCA) coherent with ENSO, IOD and SAM. In Table 1 we see that the climate indices explain a greater portion of the variability in the fire, aerosol, cloud and precipitation records for the INC region than for the NZSC region. This is likely due to the strong seasonal and monsoonal cycles in the INC. Since the NZSC is a subtropical region fluctuations in sea surface temperatures are not as drastic as in the tropics. In order to justify the removal of the climate signals the yearly AI and precipitation data are analyzed. In Figure 4 we see that when mean annual AI is plotted as a function of the normalized anomaly of precipitation El Niño or La Niña years are distinct in the INC from those that are not. As mentioned above, the influence of the climate signals in the NZSC is much weaker resulting in the less clear demarcation between years affected or not affected by an El Niño or La Niña. We also see the clear decrease in precipitation with increasing aerosol in the INC ($R = -0.67$) and a less strong relationship in the NZSC ($R = -0.27$), once the El Niño and La Niña years are removed from the linear fit calculation. Thus, all data is processed such that the climate signals are removed, as described above.

We choose not to de-trend the data since we are considering long-term changes in aerosol and precipitation and *Huang et al.* (2009b) found similar results with data that was not detrended. The final timeseries represents the residual aerosol and precipitation anomalies not explained by the climate factors. The AI and GPCP normalized anomalies are shown in Figure 5. Once climate signals are removed from both records we see that there is still a noticeable increase in AI for the later half of the N7 TOMS record in both the INC and NZSC regions. There is no obvious trend in the precipitation record for either INC or NZSC regions once the climate signals are removed.

4.4 Relationships

This section focuses on the specific relationships between AI and the various parameters available during the most recent time period focusing on AI from the OMI record (October

2004 to May 2008). It is broken down into three parts in order to understand the relationship between aerosol and fire, aerosol and cloud properities and finally aerosol and precipitation. Each section discusses the temporal relationships as well as the correlations of the means and normalized anomalies.

4.4.1 Aerosol - Fire Count

The effect of aerosol on clouds and precipitation is intimately linked to the relationship between fire occurrence and atmospheric aerosol loading. First, it is necessary to identify the timing of peak (minimum) fire occurrence and peak (minimum) aerosol. This type of analysis also helps in identifying aerosols events that are the result of dust or anthropogenic events. Figure 6 shows the mean and normalized anomaly timeseries for AI and MODIS fire counts for the INC and NZSC regions. The inter-annual variability of both AI and fire counts is clear for both the INC and NZSC regions. Figure 6a shows the temporal evolution of the mean MODIS fire count and OMI AI. We see that both OMI AI and MODIS fire counts show a seasonal pattern with strong inter-annual variability. We also note that the peak fire counts occur in September or October while the AI peak lags by one month occurring in October or November. This lag may be due in part to the tropospheric response time to aerosols, which is on the order of 1-2 months as well as the time required for aerosol to loft to heights observable by the OMI instrument (*Torres et al., 1998; de Graaf et al., 2005*). In the INC region July-December of 2006 and 2007 are similar with maximum mean fire counts of ~ 30 in September, while 2005 shows a different pattern with no main peak in fire activity. When considering the normalized anomalies of AI and fire count, Figure 6b, we see that the time series show good agreement, with a slight difference during 2006. In 2006, which is characterized by low AI and high fire counts, may have resulted from high individual fire counts combined with limited or decreased availability of fuel after the intense 2004-2005 fire season. In Figure 6c we see the clear seasonality of AI from both dust and fire in the NZSC region with the dust peak occurring primarily in July while the fire peak

varies, though occurs during austral summer (December-March). The NZSC has a fairly steady fire count cycle with annual mean maximums of ~ 10 (lower inter-annual variability than for the INC), except for 2007 in which the maximum mean fire counts double to ~ 20 . The normalized anomalies for the NZSC region, Figure 6d, show good agreement for the same time periods as in the INC. The timeseries suggest a positive relationship between fire occurrence and aerosol amount. If we consider the INC region for October 2004 through May 2008 the correlations, not shown, between the normalized anomalies of AI and fire count reveal a stronger correlation when considering fire seasons only ($R = 0.64$) than compared to full year ($R = 0.31$). In the NZSC the correlations remain the same ($R = 0.56$) for both full year and fire season only comparisons. This can be explained by the influence of dust from the central desert impacting the NZSC year round, dominating the AI signal. Again, differences between regions can partially be explained by the inclusion of dust in the NZSC samples and the observed one month time lag between peak fire counts and peak AI in the INC.

4.4.2 Aerosol - Cloud Relationships

Here we investigate the relationship and timing of maximum and minimum aerosol and fluctuations in cloud properties to understand how changes in aerosol may induce changes in cloud properties. Figure 7 shows the mean and normalized anomaly timeseries of AI and MODIS r_e for the INC and NZSC regions. The inter-annual variability of both AI and r_e is clear for both the INC and NZSC regions. Figure 7a shows the temporal evolution of the mean MODIS r_e and OMI AI. Both OMI AI and MODIS r_e show a seasonal pattern with strong inter-annual variability. The maximum r_e occurs in April during the AI minimum. The minimum r_e occurs in September, while the AI peak lags by one month occurring in October or November. When considering the normalized anomalies of AI and r_e , Figure 7b shows an anti-correlated relationship, with increases in AI corresponding to decreases in r_e ($R = -0.35$). In Figure 7c, keeping in mind that the peak dust occurs in July and the fire

297 season December-March, the NZSC is typified by a steady r_e annual cycle with annual mean
 298 maximums occurring in July during the peak in dust and minimums occurring during peak
 299 fire activity. Note that while the mean AI and r_e related to dust show positive agreement,
 300 the aerosol peaks due to fire are anti-correlated with r_e . The normalized anomalies for the
 301 NZSC region, Figure 7d, show good agreement and are not strongly influenced by the biomass
 302 burning derived aerosol. Overall, these timeseries suggest a negative relationship between r_e
 303 and aerosol amount when the aerosol is derived from biomass burning events and a positive
 304 relationship if the aerosol is derived from dust events. If we consider data only from October
 305 2004 through May 2008 the correlations, not shown, between the normalized anomalies of AI
 306 and r_e reveal a stronger correlation in the INC ($R = -0.35$) than in the NZSC ($R = -0.29$).
 307 As with fire counts, differences in correlations can be explained by weaker seasonality and
 308 the inclusion dust in the NZSC samples as well as the time lag between peak fire counts and
 309 peak AI in the INC.

310 As with r_e , MODIS CF and ISCCP MCA show distinct seasonality and excellent agree-
 311 ment ($R = 0.97$) in the INC (Figure 8a), and weak seasonality and poor agreement ($R = 0.30$)
 312 in the NZSC (Figure 8c). For the INC, peak CF and MCA occur 2-4 months (December-
 313 March) after the peak in aerosol (September-October). Figure 8b and d show the timeseries
 314 of AI, CF and MCA normalized anomalies for the INC and NZSC. In the INC, normalized
 315 anomalies of CF and AI appear to be correlated in 2005, and then anti-correlated for 2006-
 316 2008 resulting in very weak relationship ($R = 0.009$), MCA and AI are anti-correlated in
 317 2005 and correlated for 2006-2008, with an overall poor, but slightly negative, correlation
 318 ($R = -0.13$) while INC CF and MCA normalized anomalies are poorly correlated with each
 319 other ($R = -0.23$). In the NZSC normalized anomalies of MCA, CF and AI show similar
 320 trends with poor correlations ($R = 0.15$ for AI and CF, $R = -0.17$ for AI and MCA), while
 321 the NZSC CF and MCA normalized anomalies are well correlated with each other ($R =$
 322 0.91). Differences in the anomalies may partially due to the length of the data records used
 323 to calculate the anomalies (300 months for ISCCP vs 90 months for MODIS).

4.4.3 Aerosol - Cloud - Precipitation Relationships

Here we present an analysis of the observed relationship between monthly AI and precipitation. For the INC region the monthly domain-averaged normalized AI and GPCP anomalies are negatively correlated ($R = -0.16$) when considering the entire data record and sorted by season (Figure 9a-e). For the INC, the correlations are greatest during austral spring (SON, $R = -0.16$) and fall (MAM, $R = -0.16$) when there is adequate precipitation and aerosol. During the peak northern fire season, SON, we see the least scatter and the lowest variability. The correlations are weaker during austral winter (JJA, $R = -0.13$), when precipitation begins decreasing before the initiation of the main fire season in austral summer (DJF, $R = -0.14$) during the monsoon season when precipitation increases dramatically and aerosol production is at a minimum. The combinations of low precipitation with low aerosol (JJA) and high precipitation with very low aerosol (DJF) result in weaker relationships between AI and GPCP. For the NZSC, there is no clear relationship between AI and GPCP precipitation when looking at the entire record or seasonally (Figure 10a-e). For all months and seasons GPCP precipitation over the NZSC region shows more variability than AI. For each, inter-annual variability for each month plays a large role in determining the scatter and the resulting correlation coefficient.

5 Summary and Discussion

In this study, we have used a combination of satellite datasets for both the present (MODIS) and the recent past (TOMS, OMI, GPCP and ISCCP) to look at the relationships between aerosols, clouds and precipitation in Australia. We find that atmospheric aerosol loading changes on annual, inter-annual and decadal timescales in the Australian region. On the decadal timescale we see a general increase in AI over the entire region (both the INC and NZSC). Inter-annual variations in AI are influenced by El Niño, SAM and IOD, though in varying amounts depending on the region, and must be removed in order to separate the ef-

fects of meteorology and dynamics from the influence of aerosols on precipitation and cloud properties. Annual variations in AI manifest as changes in the timing of the fire season and its length, which has been increasing over the study period. In contrast, we find that precipitation in the Australian region has remained fairly constant on a decadal time scale while, like AI, it varies as a result of El Niño, SAM and IOD on the inter-annual timescale. The annual precipitation cycle (timing of maximum and minimum precipitation) is found to be relatively stable regardless of the inter-annual influences. We find that increased fire occurrence positively correlates with increased aerosol loading and occurs during annual precipitation minimums. Unfortunately, since MODIS measures the number of fires rather than the fire intensity correlations appear weaker than expected. We find that the maximum aerosol loading occurs approximately one month after the peak in fire counts. This is likely due to the average residence time of biomass burning aerosol and the time required for transport to upper levels of the troposphere. In the most recent time period (2002 to the 2008) cloud r_e and CF, like precipitation, maintain relatively stable annual cycles (especially in the INC) with little variation in the timing of maximums and minimums. The southern NZSC region shows more annual and inter-annual variability in CF than in the north. Counter-intuitively, peak aerosol appears to occur after the minimum in r_e , as with fire counts. Note that changes to clouds would occur in the lower troposphere, soon after the aerosols are emitted (i.e. closer to actual fire occurrence). In the case of the aerosol loading it takes approximately one month for the peak aerosol to occur after the peak fire counts. This accumulation time would offset the maximum AI from the corresponding, relatively immediate, effects on cloud properties such as changes in r_e and CF. Fire count and r_e are anti-correlated, and in general, years with weak fire seasons such as 2006 have larger effective radii in the following wet season.

The main results from this study are as follows. The choice of region (dynamic and meteorologic setting) is important in determining the relationships between aerosols, clouds and precipitation. We find that the strength of the negative correlation between AI and precipi-

tation is dependent on the dynamic setting, such that the northern INC region, dominated by convective clouds, shows a stronger decrease in precipitation with increasing aerosol. In the southern NZSC region, clouds which are predominately the result of subsidence or storm tracks show a weaker response to aerosol. Thus, global generalizations of the relationships between changes in aerosol loading and the effect on precipitation amount cannot be made without taking regional differences into consideration.

In summary, the longer time records used in this study show evidence of ongoing inter-decadal and inter-annual variations. It is possible that changes in climate, not accounted for by the El Niño, SAM and IOD indices may be playing a role as well. It is likely that changes in the length of the fire season over the last decade is contributing to the overall increase in aerosol loading. In general, we find that the relationships between aerosols, precipitation and clouds do not change on the decadal or inter-annual timescales. Of course, caution needs to be exercised when interpreting the results due to the uncertainties inherent in satellite derived aerosol, cloud and precipitation retrievals. The observed relationships and correlations between aerosol, precipitation and cloud properties could also be due to correlative biases in the satellite retrieved datasets, though since we use different datasets on different platforms over a time period of 30 years, the likelihood of this is reduced. Since we did not sort individual grid boxes by dynamical regime the results shown here can be due to meteorology driving both aerosols, clouds and precipitation. Future work, sorting these data sets by dynamical properties such as vertical velocities and lower tropospheric stability and meteorological properties such as cloud liquid water content, is necessary since correlation does not imply causality.

Acknowledgments

This work was performed at the Jet Propulsion Laboratory, California Institute of Technology, under contract with NASA. We thank the support by NASA Atmospheric Composition

401 Modeling Analysis Program (ACMAP), Interdisciplinary (IDS) Research in Earth Sciences
402 program, and the Aura project. we thank Omar Torres for help with the OMI data and
403 useful discussions during manuscript preparations.

References

- Andreae, M. O., D. Rosenfeld, P. Artaxo, A. A. Costa, G. P. Frank, K. M. Longo, and M. A. F. Silva-Dias (2004), Smoking rain clouds over the amazon, *Science*, *303*, 1337–1342.
- Bell, T. L., D. Rosenfeld, K.-M. Kim, J.-M. oo, M.-I. Lee, and M. Hahnenberger (2008), Midweek increase in U.S. summer rain and storm heights suggest air pollution invigorates rainstorms, *J. Geophys. Res.*, *113*, DOI: 10.1029/2007JD008623.
- Bowman, D. M. J. S., and B. A. Wilson (1988), Fuel characteristics of coastal monsoon forests, Northern Territory, Australia, *J. Biogeography*, *5/6*, 807–817.
- Chu, D. A., Y. J. Kaufman, C. Ichoku, L. A. Remer, D. Tanre, and B. N. Holben (2002), Validation of MODIS aerosol optical depth retrieval over land, *Geophys. Res. Lett.*, *29*, DOI: 10.1029/2001GL013205.
- Chu, D. A., Y. J. Kaufman, G. Zibordi, J. D. Chern, J. Mao, C. Li, and B. N. Holben (2003), Global monitoring of air pollution over land from the Earth Observing System-Terra Moderate Resolution Imaging Spectroradiometer (MODIS), *J. Geophys. Res.*, *108*, DOI: 10.1029/2002JD003179.
- de Graaf, M., P. Stammes, O. Torres, and R. Koelemeijer (2005), Absorbing aerosol index: Sensitivity analysis, application to gome and comparison with toms, *J. Geophys. Res. - Atmos.*, *110*, doi: 10.1029/2004JD005178.
- Denman, K., et al. (2007), *Climate Change 2007: The Physical Science Basis. Contribution of Working Group I to the Fourth Assessment Report of the Intergovernmental Panel on Climate Change*, chap. Couplings Between Changes in the Climate System and Biogeochemistry, Cambridge University Press, Cambridge, United Kingdom and New York.

427 Feingold, G., and H. Siebert (2009), *Strungmann Forum*, vol. 2, chap. Chapter 14, Cloud-
428 aerosol interactions from the micro to the cloud scale, pp. 321–338, The MIT press.

429 Gentilli, J. (1971), *World Survey of Climatology*, chap. Climates of Australia and New
430 Zealand, p. 84, Elsevier.

431 Graf, H.-F., J. Yang, and T. M. Wagner (2009), Aerosol effects on clouds and precipitation
432 during the 1997 smoke episode in Indonesia, *Atmos. Chem. Phys.*, *9*, 743–756.

433 Gunn, R., and B. B. Phillips (1957), An experimental investigation of the effect of air
434 pollution on the initiation of rain, *J. Meteor.*, *14*, 272–280.

435 Hendon, H. H., D. W. J. Thompson, and M. C. Wheeler (2007), Australian rainfall and
436 surface temperature variations associated with the Southern Hemisphere Annular mode,
437 *J. Clim.*, *20*, DOI: 10.1175/JCLI4134.1.

438 Hennessy, K., C. Lucas, N. Nicholls, J. Bathols, R. Suppiah, and J. Ricketts (2005), Climate
439 change impacts on fire-weather in south-east Australia, *Tech. rep.*, CSIRO Marine and
440 Atmospheric Research Bushfire CRC and Australia Bureau of Meteorology.

441 Herman, J. R., P. K. Bhartia, O. Torres, C. Hsu, C. Seftor, and E. Celarier (1997), Global
442 distribution of UV-absorbing aerosols from Nimbus7/TOMS data, *J. Geophys. Res.*, *102*,
443 16,911–16,922.

444 Hsu, N. C., J. R. Herman, P. K. Bhartia, C. J. Seftor, O. Torres, A. M. Thompson, J. F.
445 Gleason, and B. N. Eck, T. F. and Holben (1996), Detection of biomass burning smoke
446 from TOMS measurements, *Geophys. Res. Lett.*, *23*, 745–748.

447 Huang, J., C. Zhang, and P. J. M. (2009a), African aerosol and large-scale precipitation
448 variability over West Africa, *Environ. Res. Lett.*, *4*, DOI: 10.1088/1748-9326/4/1/015006.

- Huang, J., C. Zhang, and J. M. Prospero (2009b), Large-scale effect of aerosols on precipitation in the West African Monsoon region, *Q. J. R. Meteorol. Soc.*, *135*, DOI: 10.1002/qj.391.
- Huffman, G. J., R. F. Adler, D. T. Bolvin, and G. Gu (2009), Improving the global precipitation record: GPCP Version 2.1, *Geophys. Res. Lett.*, *36*, DOI: 10.1029/2009GL040000.
- Jiang, J. H., H. Su, M. R. Schoeberl, S. T. Massie, P. Colarco, S. Platnick, and N. J. Livesey (2008), Clean and polluted clouds: Relationships among pollution, ice, clouds, and precipitation in south america, *Geophys. Res. Lett.*, *35*, DOI: 10.1029/2008GL03431.
- Jiang, J. H., H. Su, C. Zhai, S. T. Massie, M. R. Schoeberl, P. R. Colarco, S. Platnick, Y. Gu, and K.-N. Lious (2010), Influence of convection and aerosol pollution on ice cloud particle effective radius, *Atmos. Chem. Phys. Discuss.*, *10*, doi:10.5194/acpd-10-23091-2010.
- Kaufman, Y. J., D. Tanre, L. A. Remer, E. F. Vermote, and A. Chu (1997), Operational remote sensing of tropospheric aerosol over land from EOS moderate resolution imaging spectrometer., *J. Geophys. Res.*, *102*, 17,051–67.
- Levelt, P. F., G. H. J. van den Oord, M. R. Dobber, A. Malkki, H. Visser, J. de Vries, P. Stammes, J. O. V. Lundell, and H. Saari (2006), The ozone monitoring instrument, *IEEE Trans. Geosci. Remote Sens.*, *44*, DOI: 10.1109/TGRS.2006.872336.
- Lin, J. C., T. Matsui, R. A. Pielke Sr., and C. Kummerow (2006), Effects of biomass-burning-derived aerosols on precipitation and clouds in the Amazon Basin: a satellite-based empirical study, *J. Geophys. Res.*, *111*, DOI: 10.1029/2005JD006884.
- Lu, M.-L., G. Feingold, H. H. Jonsson, P. Y. Chuang, H. Gates, R. C. Flagan, and J. H. Seinfeld (2008), Aerosol-cloud relationships in continental shallow cumulus, *J. Geophys. Res.*, *113*, DOI: 10.1029/2007JD009354.

- Lucas, C., K. Hennessy, G. Mills, and J. Bathols (2007), Bushfire weather in southeast australia: Recent trends and projected climate change impacts, *Tech. rep.*, Consultancy report by CSIRO Marine and Atmospheric Research, Bureau of Meteorology and Bush Fire CRC.
- Marshall, G. J. (2003), Trends in the Southern Annular Mode from observations and reanalysis, *J. Clim.*, *16*, 4134–4143.
- Martins, J. A., and M. A. F. Silva Dias (2009), The impact of smoke from forest fires on the spectral dispersion of cloud droplet size distributions in the Amazonian region, *Environ. Res. Lett.*, *4*, DOI: 10.1088/1748-9326/4/1/015002.
- Marx, S. K., B. S. Kamber, and H. A. McGowan (2005), Estimates of australian dust flux into new zealand: Quantifying the eastern australian dust plume pathway using trace element calibrated 210pb as a monitor, *Earth and Planetary Sci. Lett.*, *239*, 336–351.
- Mitchell, R. M., S. K. Campbell, and Y. Qin (2010), Recent increase in aerosol loading over the australian arid zone, *Atmos. Chem. Phys.*, *10*, 1689–1699.
- Murphy, B. F., and B. Timbal (2008), A review of recent climate variability and climate change in southeastern australia, *Int. J. Clim.*, *28*, DOI: 10.1002/joc.1627.
- Nicholls, N. (1989), Sea surface temperatures and australian droughts, *J. Clim.*, *9*, 965–973.
- Pawlowska, H., W. W. Grabowski, and J.-L. Brenguier (2006), Observations of the width of the cloud droplet spectra in stratocumulus, *Geophys. Res. Lett.*, *33*, DOI: 10.1029/2006GL026841.
- Ramanathan, V., P. J. Crutzen, J. T. Kiehl, and D. Rosenfeld (2001), Aerosols, climate, and the hydrolgical cycle, *Science*, *294*, DOI: 10.1126/science.1064034.
- Remer, L. A., et al. (2002), Validation of modis aerosol retrieval over ocean, *Geophys. Res. Lett.*, *29*, DOI 10.1029/2001GL013204.

- Reynolds, R. W., and T. M. Smith (1994), Improved global sea surface analyses using optimum interpolation, *J. Clim.*, 7, 929–948.
- Rosenfeld, D. (1999), TRMM observed first direct evidence of smoke from forest fires inhibiting rainfall, *Geophys. Res. Lett.*, 26, 3105–3108.
- Rosenfeld, D., U. Lohmann, G. B. Raga, C. D. O’Dowd, M. Kulmala, S. Fuzzi, A. Reissell, and M. O. Andreae (2008), Flood or drought: How do aerosols affect precipitation?, *Science*, 321, DOI: 10.1126/science.1160606.
- Rossow, W. B., and R. A. Schiffer (1991), ISCCP cloud data products, *Bull. Amer. Meteor. Soc.*, 72, 2–20.
- Rossow, W. B., and R. A. Schiffer (1999), Advances in understanding clouds from ISCCP, *Bull. Amer. Meteor. Soc.*, 80, 2261–2287.
- Saji, N. H., B. N. Goswami, P. N. Vinayachandran, and Y. Tamagata (1999), A dipole mode in the tropical Indian Ocean, *Nature*, 401, 360–363.
- Specht, R. L. (1970), *The Australian Environment*, chap. Vegetation, pp. 44–67, Melbourne University Press, Melbourne, Australia.
- Taschetto, A. D., and M. H. England (2009), El Niño Modoki impacts on Australian rainfall, *J. Clim.*, 22, DOI: 10.1175/2008JCLI2589.1.
- Torres, O., P. K. Bhartia, J. R. Herman, and Z. Ahmad (1998), Derivation of aerosol properties from satellite measurements of backscattered ultraviolet radiation. Theoretical basis, *J. Geophys. Res.*, 103, 17,099–17,110.
- Torres, O., P. K. Bhartia, J. Herman, A. Sinyuk, and B. Holben (2002), A long term record of aerosol optical thickness from TOMS observations and comparison to AERONET measurements, *J. Atm. Sci.*, 59, 398–413.

519 Twomey, S. (1974), Pollution and planetary albedo, *Atmos. Env.*, *8*(12), 1251–1256.

520 Ummenhofer, C. C., M. H. England, P. C. McIntosh, G. A. Meyers, M. J. Pook, J. S.
521 Risbey, A. S. Gupta, and A. S. Taschetto (2009a), What causes southeast Australia’s
522 worst droughts?, *Geophys. Res. Lett.*, *36*, doi:10.1029/2008GL036801.

523 Ummenhofer, C. C., A. S. Gupta, A. S. Taschetto, and M. H. England (2009b), Modula-
524 tion of Australian precipitation by meridional gradients in East Indian Ocean sea surface
525 temperature, *J. Clim.*, *22*, 5597–5610.

526 Verdon-Kidd, D. C., and A. S. Kiem (2009), Nature and causes of protracted droughts in
527 southeast Australia: Comparison between the Federation, WWII, and Big Dry droughts,
528 *Geophys. Res. Lett.*, *36*, doi:10.1029/2009GL041067.

529 Wyser, K. (1998), The effective radius in large-scale models: impact of aerosols and coales-
530 cence, *Atmos. Res.*, *49*, 213–234.

531 Zhang, R., G. Li, J. Fan, D. L. Wu, and M. J. Molina (2007), Intensification of Pacific storm
532 track linked to Asian pollution, *Proc. Nat. Acad. Sci.*, *104*, 10.1073/pnas.0700618104.

Figure Captions

Figure 1: Indonesian and Northern Coast (INC) study region encompasses -0.5 to -20.5 (°S) and 90.625 to 178.125 (°W). New Zealand and Southern Coast (NZSC) study region encompasses -30.5 to -50.5 (°S) and 90.625 to 178.125 (°W). Both regions include data retrieved over land and ocean.

Figure 2: Monthly mean timeseries of a) TOMS/OMI AI for INC (red) and NZSC (blue), b) GPCP precipitation for INC (red) and NZSC (blue), c) Nino3.4 index, d) IOD, and e) 3-month smoothed SAM. For climate indices blue shading indicates periods of potentially above average precipitation while brown shading indicates periods of potentially below average precipitation. The three satellite data records, N7 TOMS, EP TOMS and OMI, are denoted by the arrows. Grey shading corresponds to strong El Niño years.

Figure 3: a) Study regions and climatological mean of MODIS fire counts (number of fires, colors), b) annual cycles of fire count with standard deviations for INC and NZSC regions, c) aerosol index (AI, unit less, colors) using TOMS and OMI datasets, d) annual cycles of AI for Nimbus-7 TOMS, Earth Probe TOMS and OMI and the three satellite mean for INC and NZSC regions, e) same as in a) but for MODIS cloud fraction (colors), f) annual cycle of cloud fraction with standard deviations for INC and NZSC regions, g) same as in a) but for GPCP precipitation (cm/month, colors), h) annual cycle of GPCP precipitation for INC and NZSC regions. For all annual cycles red curves are for INC and blue curves are for NZSC region.

Figure 4: Scatterplots of the yearly averaged mean AI and GPCP normalized anomalies (climate signals not removed); INC region ($R_{INC} = -0.67$, $n = 18$); b) NZSC region ($R_{NZSC} = -0.27$, $n = 18$). El Niño and La Niña years in gray markers, all other data in black markers. Red lines indicate linear regression fits for data from years that are not classified as El Niño or La Niña.

Figure 5: Timeseries of normalized anomalies of AI and GPCP precipitation for INC

region (red) and NZSC region (blue). Thin lines are monthly values while thicker lines are three-month smoothed data. Satellite sampling periods are denoted by the arrows.

Figure 6: Timeseries of a) monthly mean values and b) normalized anomalies of AI (red) and MODIS Fire Counts (brown) for the INC Region; c) monthly mean values and d) normalized anomalies of AI (blue) and MODIS Fire Counts (brown) for the NZSC Region.

Figure 7: Timeseries of a) monthly mean values and b) normalized anomalies of AI (red) and MODIS r_e (green) for the INC Region; c) monthly mean values and d) normalized anomalies of AI (blue) and MODIS r_e (green) for the NZSC Region.

Figure 8: Timeseries of a) monthly mean values and b) normalized anomalies of AI (red), MODIS Cloud Fraction (black), and ISCCP Mean Cloud Amount (gray) for the INC Region; c) monthly mean values and d) normalized anomalies of AI (blue) and MODIS Cloud fraction (black) and ISCCP Mean Cloud Amount (gray) for the NZSC Region. Note that ISCCP data are scaled by 0.01 to match MODIS data format.

Figure 9: Scatterplots of the INC domain averaged AI and GPCP normalized anomalies; a) All months ($R_{INC} = -0.16$, $n = 294$), b) DJF ($R = -0.14$, $n = 74$); c) MAM ($R = -0.16$, $n = 74$); d) JJA ($R = -0.13$, $n = 72$); e) SON ($R = -0.16$, $n = 74$). Solid black lines indicate linear regression fits.

Figure 10: Scatterplots of the INC domain averaged AI and GPCP normalized anomalies; a) All months ($R_{NZSC} = 0.05$, $n = 293$), b) DJF ($R = -0.02$, $n = 74$); c) MAM ($R = -0.03$, $n = 74$); d) JJA ($R = 0.10$, $n = 72$); e) SON ($R = -0.002$, $n = 73$). Solid black lines indicate linear regression fits. Note, for All Seasons and SON the September outlier was removed from the linear regression fit calculations.

Tables

Region	Fire Count	N7	EP	OM	GPCP	r_e	CF	MCA
INC	24%	12%	24%	10%	10%	19%	24%	12%
NZSC	10%	6%	3%	16%	4%	4%	3%	4%

Table 1: R^2 values from linear regression of Nino3.4, IOD and SAM climate indices.

Dates	Region	Satellite	Mean $\pm \sigma$ (unit less)
11/1978 to 4/1993	INC	N7 TOMS	0.71 ± 0.10
	NZSC	N7 TOMS	0.68 ± 0.09
7/1996 to 11/2001	INC	EP TOMS	0.75 ± 0.10
	NZSC	EP TOMS	0.70 ± 0.06
10/2004 to 5/2008	INC	OMI	0.76 ± 0.07
	NZSC	OMI	0.79 ± 0.10

Table 2: Mean AI values for each satellite

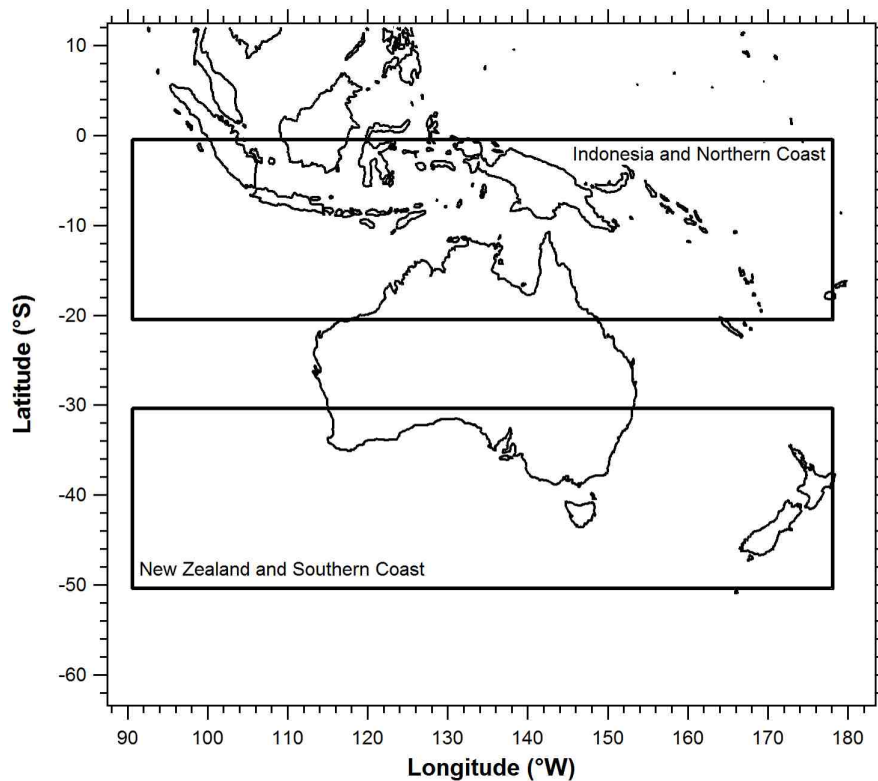


Figure 1: Study Regions. Indonesian and Northern Coast (INC) study region encompasses - 0.5 to -20.5 (°S) and 90.625 to 178.125 (°W). New Zealand and Southern Coast (NZSC) study region encompasses -30.5 to -50.5 (°S) and 90.625 to 178.125 (°W). Both regions include data retrieved over land and ocean.

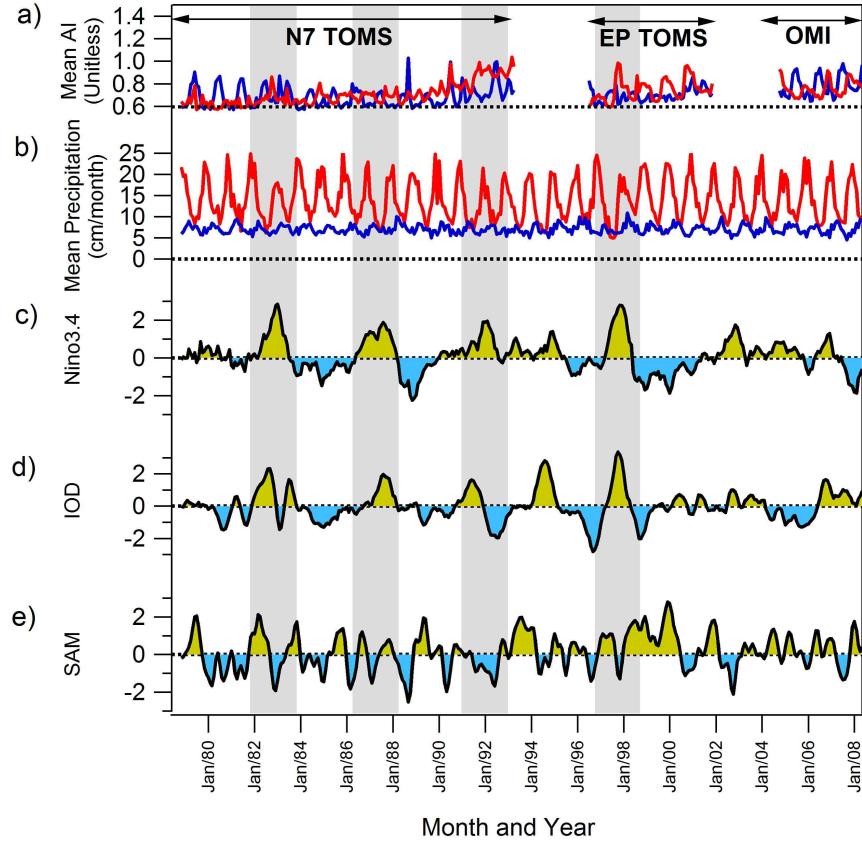


Figure 2: Monthly mean timeseries of a) TOMS/OMI AI for INC (red) and NZSC (blue), b) GPCP precipitation for INC (red) and NZSC (blue), c) Nino3.4 index, d) IOD, and e) 3-month smoothed SAM. For climate indices blue shading indicates periods of potentially above average precipitation while brown shading indicates periods of potentially below average precipitation. The three satellite data records, N7 TOMS, EP TOMS and OMI, are denoted by the arrows. Grey shading corresponds to strong El Niño years.

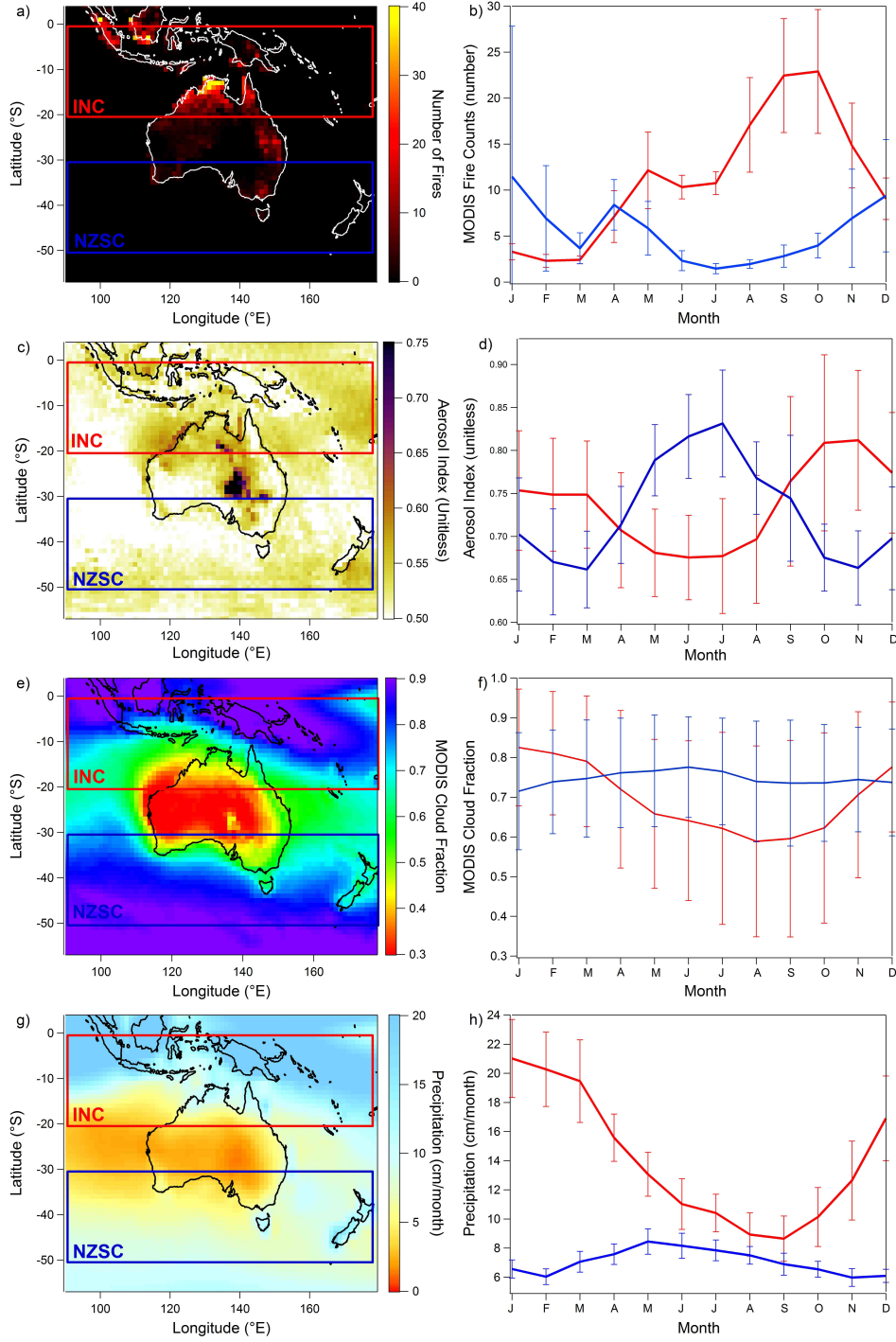


Figure 3: Climatologies and annual cycles. a) Study regions and climatological mean of MODIS fire counts (number of fires, colors), b) annual cycles of fire count with standard deviations for INC and NZSC regions, c) aerosol index (AI, unit less, colors) using TOMS and OMI datasets, d) annual cycles of AI for Nimbus-7 TOMS, Earth Probe TOMS and OMI and the three satellite mean for INC and NZSC regions, e) same as in a) but for MODIS cloud fraction (colors), f) annual cycle of cloud fraction with standard deviations for INC and NZSC regions, g) same as in a) but for GPCP precipitation (cm/month, colors), h) annual cycle of GPCP precipitation for INC and NZSC regions. For all annual cycles red curves are for INC and blue curves are for NZSC region.

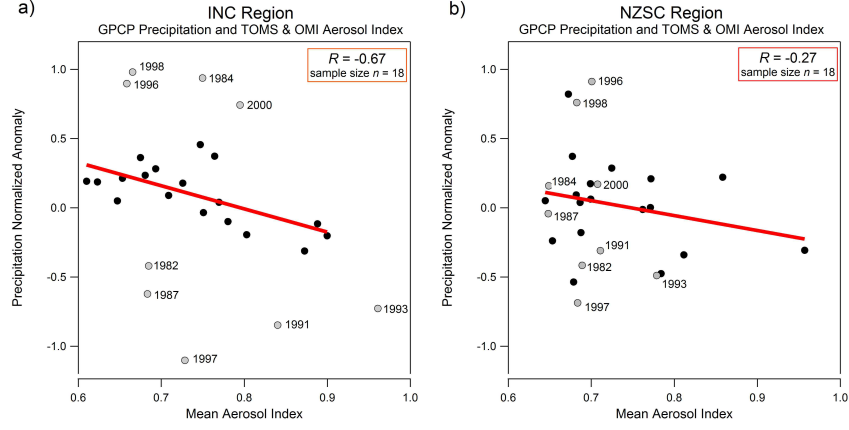


Figure 4: Mean AI and normalized precipitation anomaly comparisons. Scatterplots of the yearly averaged mean AI and GPCP normalized anomalies (climate signals not removed); INC region ($R_{INC} = -0.67$, $n = 18$); b) NZSC region ($R_{NZSC} = -0.27$, $n = 18$). El Niño and La Niña years in gray markers, all other data in black markers. Red lines indicate linear regression fits for data from years that are not classified as El Niño or La Niña.

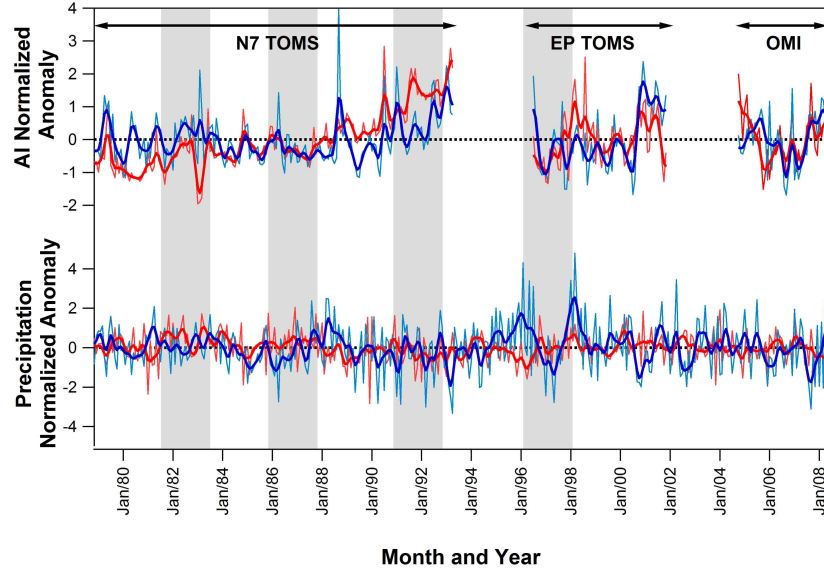


Figure 5: Timeseries of normalized anomalies of AI and GPCP precipitation for INC region (red) and NZSC region (blue). Thin lines are monthly values while thicker lines are three-month smoothed data. Satellite sampling periods are denoted by the arrows.

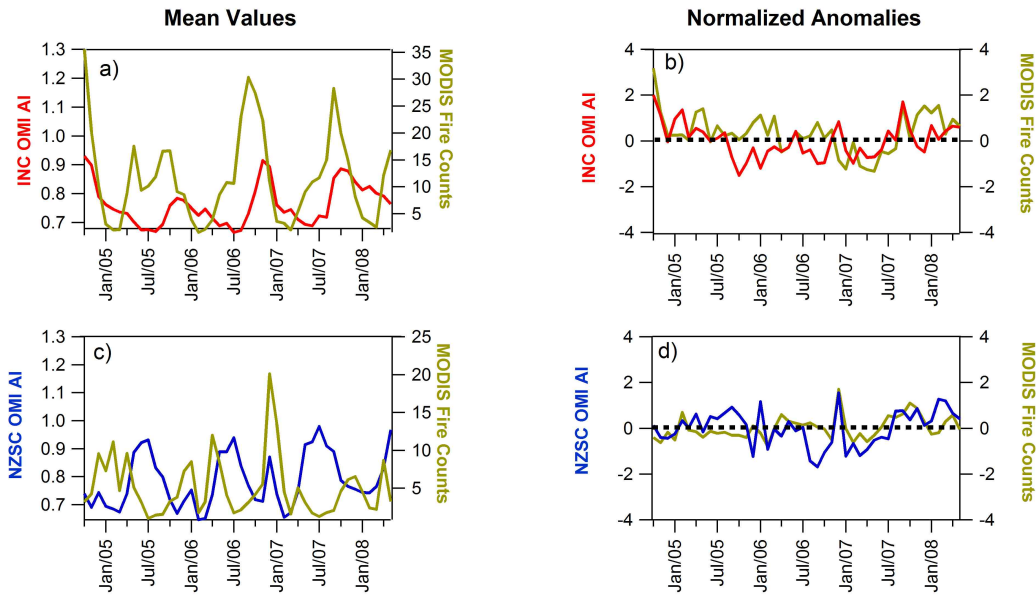


Figure 6: Timeseries comparisons for OMI AI and MODIS fire count. Timeseries of a) monthly mean values and b) normalized anomalies of AI (red) and MODIS Fire Counts (brown) for the INC Region; c) monthly mean values and d) normalized anomalies of AI (blue) and MODIS Fire Counts (brown) for the NZSC Region.

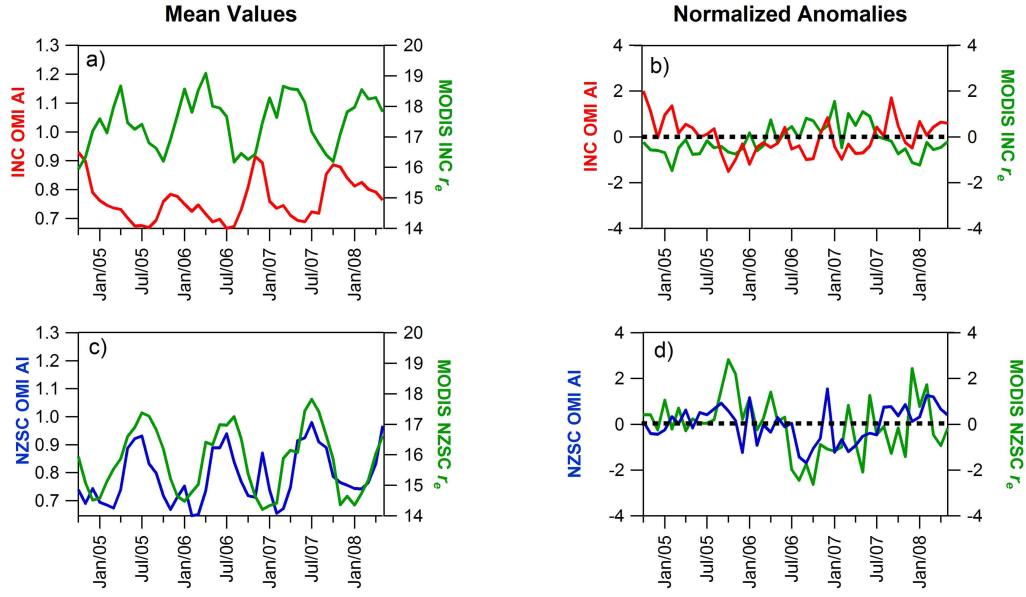


Figure 7: Timeseries comparison of OMI AI and MODIS r_e . Timeseries of a) monthly mean values and b) normalized anomalies of AI (red) and MODIS r_e (green) for the INC Region; c) monthly mean values and d) normalized anomalies of AI (blue) and MODIS r_e (green) for the NZSC Region.

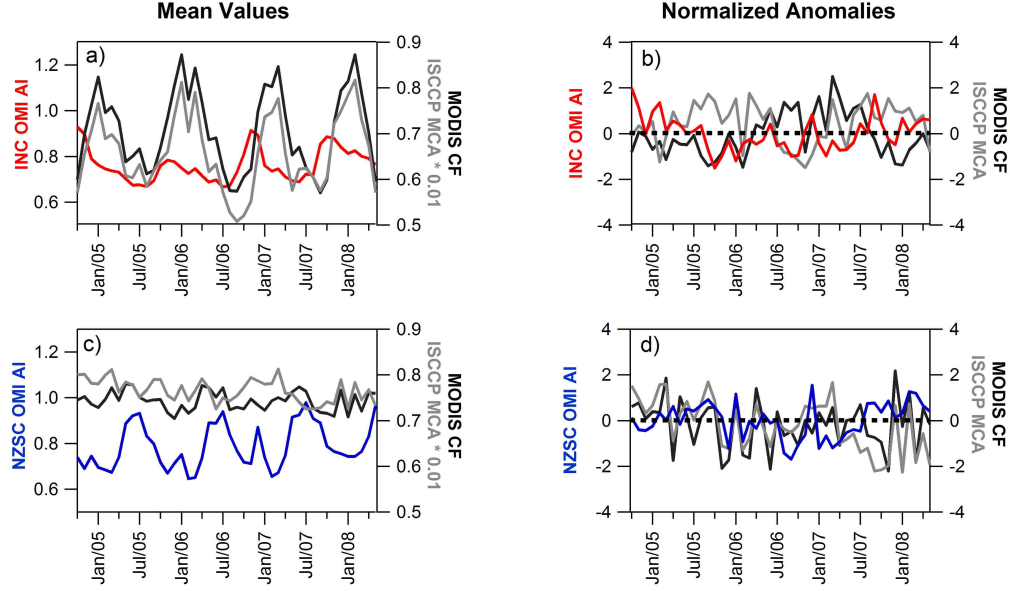


Figure 8: Timeseries comparison of OMI AI, MODIS CF and ISCCP MCA. Timeseries of a) monthly mean values and b) normalized anomalies of AI (red), MODIS Cloud Fraction (black), and ISCCP Mean Cloud Amount (gray) for the INC Region; c) monthly mean values and d) normalized anomalies of AI (blue) and MODIS Cloud fraction (black) and ISCCP Mean Cloud Amount (gray) for the NZSC Region. Note that ISCCP data are scaled by 0.01 to match MODIS data format.

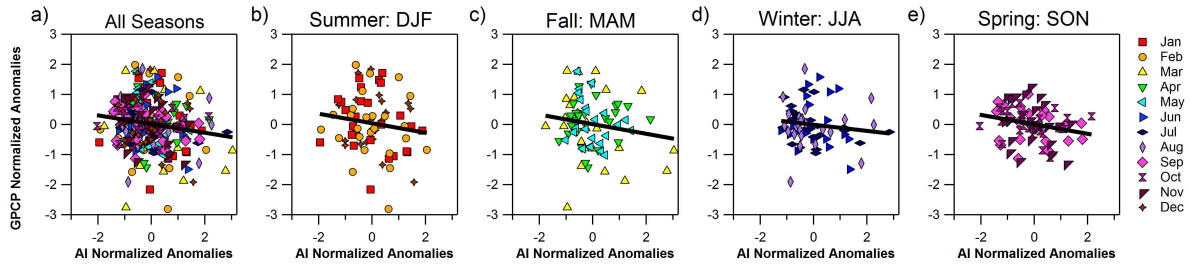


Figure 9: INC seasonal comparisons of AI and GPCP. Scatterplots of the INC domain averaged AI and GPCP normalized anomalies; a) All months ($R_{INC} = -0.16$, $n = 294$), b) DJF ($R = -0.14$, $n = 74$); c) MAM ($R = -0.16$, $n = 74$); d) JJA ($R = -0.13$, $n = 72$); e) SON ($R = -0.16$, $n = 74$). Solid black lines indicate linear regression fits.

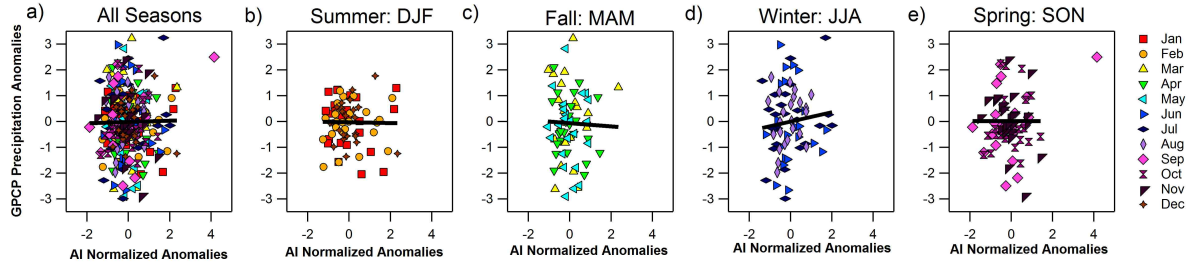


Figure 10: NZSC seasonal comparisons of AI and GPCP. Scatterplots of the INC domain averaged AI and GPCP normalized anomalies; a) All months ($R_{NZSC} = 0.05$, $n = 293$), b) DJF ($R = -0.02$, $n = 74$); c) MAM ($R = -0.03$, $n = 74$); d) JJA ($R = 0.10$, $n = 72$); e) SON ($R = -0.002$, $n = 73$). Solid black lines indicate linear regression fits. Note, for All Seasons and SON the September outlier was removed from the linear regression fit calculations.